SPH simulation of diffusion and coupled concentration dependent ionic migration with precipitation and dissolution

Andrew Cannon
Mechanical Engineering Department
Boston University
Boston, MA
AndrewCa@bu.edu

Emily Ryan
Mechanical Engineering Department
Boston University
Boston, MA
RyanEm@bu.edu

Abstract—
An SPH model has been developed to study interfacial stability in lithium metal batteries at the anode/electrolyte interface. A major challenge in lithium metal batteries is the formation of dendrites at the interface due to uneven stripping and plating of lithium over multiple charge/discharge cycles. Dendrite nucleation is thought to occur near defects on the anode surface. The SPH model includes the effects of a spatially varying nucleation rate to simulate impurities on the anode surface and is able to simulate dendrite growth over multiple charge and discharge cycles. Charging protocols, i.e. constant voltage charging or pulsed charging, are of great interest because they allow for fast charging with fewer performance impacts. This work considers the effects of mass transport, ion diffusion, charging protocols and surface impurities on the rate of dendrite growth and the morphology of the dendrites.
The SPH model simulates the physics at the electrolyte/anode interface by solving the governing equations for diffusion, migration, and the electro-potential distribution. The equations calculate the concentration of two species (one positively and one negatively charged) in the liquid particles (electrolyte) and near a reactive, moving interface anode and dendrites surfaces.

I. INTRODUCTION

The world is transitioning to more sustainable methods of energy generation, i.e. wind and solar. These alternative energy sources suffer from tradeoffs; they do not always produce the energy when or where it is needed, making storage of this energy a high priority. Lithium ion (Li-ion) batteries have become the gold standard in portable energy storage; however, research into higher energy density storage is ongoing as Li-ion batteries are not able to meet the future demands for energy storage in areas like transportation[1].

A promising replacement for the Li-ion battery is the lithium metal battery (LMB)[2]. LMBs are of great interest because of their high specific capacity and electrochemical potential due to a pure lithium metal anode. In Li-ion batteries, lithium ions (Li^+) intercalate between graphite in the anode; while in LMBs, Li^+ are deposited directly onto the lithium metal anode. This mechanistic difference between Li-ion batteries and LMBs introduces unique challenges. The primary challenge with LMBs is dendrite growth, which occurs due to the non-uniform plating of Li^+ over multiple charge/discharge cycles. Dendrites are a challenge for two reasons: they reduce the coulombic efficiency (CE) of the battery leading to low cycle life and they cause short circuits which can lead to thermal runaway and explosions[3]. Understanding the conditions that lead to various dendrite morphologies is a critical aspect of understanding dendrite growth. Dendrite morphology effects battery performance in different ways: thin, long dendrites lead to lower CE and are more likely to pierce the battery's separator causing a short circuit; thicker, more bush-like dendrite structures cause less performance and safety issues.

The uneven deposition of Li^+ on the anode surface is due to both non-uniform transport in the electrolyte and heterogeneous surface reactions. Previous studies have investigated the effects of the battery separator on non-uniform transport in the electrolyte[4]. In this work the effects of heterogeneous surface reactions are considered. Reactions along the anode surface are regulated by the solid-electrolyte interphase (SEI) which is a thin (~10 nm)[5,6] layer comprising of various lithium compounds i.e. Li_2O, Li_2CO_3, and $LiOH$[7]. The SEI slows Li^+ transport to the anode relative to the transport in the electrolyte[8]. Unfortunately, the SEI can become unstable under mechanical stress and high surface overpotentials[9,10]. The instabilities result in cracks along the SEI, where Li^+ preferentially deposit leading to dendrite formation.

Recently, Kim et al[11] looked at methods for intentionally altering the native SEI layer in order to influence the dendrite morphology. They mechanically deformed the SEI layer by pressing a polymer mold on to the lithium metal anode to create an impression of right rectangular prisms. This process created two changes to the anode surface (in addition to the patterned surface): 1) lower surface roughness than the unaltered anode, confirmed by SEM images, and 2) the native SEI layer was disrupted especially at the bottom surface of the cavity. The second change was established by their observations that lithium was preferentially deposited in these locations. Controlling lithium deposition is of great interest because the ultimate goal is to charge LMBs without problematic dendrite growth. Building upon Kim et al's work, the research presented here examines the effects of an altered surface geometry and SEI layer on dendrite morphology under high and low charge rates. Increasing the charging rate

continues to be extremely desirable for battery systems but comes at the cost of problematic dendrite growth[12–14].
The method used for this work is a numerical study using smoothed particle hydrodynamics (SPH). SPH offers advantages over other modeling methods[15], i.e. phase-field modeling[16], primarily SPH's ability to accurately capture the morphology of dendritic growth[17]. Building upon our previously published research[18], we investigate the effects of charging rates and heterogeneous surface reactions on dendrite morphology.

II. METHODS

A. Governing equations

The SPH model simulates the physics at the electrolyte/anode interface by solving the governing equations for diffusion, migration, and electro-potential distribution using the formulation by Chazalviel[19]. Convection in the thin region along the anode surface is negligible so is not included in this version of the SPH model[20]. The SPH model calculates the diffusion and migration using the Nernst-Plank equations for the anions and cations,

$$\frac{\delta c_a}{\delta t} = D_a \Delta^2 c_a - \mu_a \nabla \cdot (c_a \nabla \boldsymbol{E}) \tag{1a}$$

$$\frac{\delta c_c}{\delta t} = D_c \Delta^2 c_c + \mu_c \nabla \cdot (c_c \nabla \boldsymbol{E}) \tag{1b}$$

where, c is the concentration, D is the diffusion coefficient, μ is the ionic mobility and $\boldsymbol{E}$ is the electric field. The subscripts a and c indicate the anion and cation species, respectively. The Poisson equation for the electrostatic potential V is

$$\Delta V = \nabla \boldsymbol{E} = -\frac{e z_c C_c - e z_a C_a}{\epsilon \epsilon_0}, \tag{2}$$

where ez_c and ez_a is the cation and anion electric charge, ϵ_0 is the vacuum permittivity and ϵ is the permittivity constant of the electrolyte.
A first order reactive boundary condition,

$$D_c \Delta^2 c_c + \mu_c \nabla \cdot (c_c \nabla \boldsymbol{E}) = k\left(c_c - c_{eq,c}\right), \tag{3}$$

controls the dendrite growth and dissolution process at the anode surface and subsequent reactive interface. The reaction rate coefficient k can vary at different locations inside the simulation domain and $c_{eq,c}$ controls the charging and discharging condition of the battery simulation. During charging $c_{eq,c}$ is lower than c_0 and higher during discharging. At the anode/dendrite surface, the boundary condition for anions is

$$D_a \Delta^2 c_a - \mu_a \nabla \cdot (c_a \nabla \boldsymbol{E}) = 0 \tag{4}$$

because anions do not participate in the dendrite growth reaction.

B. Numerical Implementation

The governing equations are modeled using SPH. The SPH discretization for the Nernst-Plank equation for the cation transport is

$$\frac{\mathrm{D}C_{c,i}}{\mathrm{D}t} = \sum_{j \in fluid} \frac{2 D_c m_j \overrightarrow{r_{ij}}}{\rho_j \left(\overrightarrow{r_{ij}}\right)^2} \left(C_{c,i} - C_{c,j}\right) \nabla W\left(\overrightarrow{r_{ij}}, h\right) + \sum_{j \in fluid} \frac{m_j \overrightarrow{r_{ij}}}{\rho_j \left(\overrightarrow{r_{ij}}\right)^2} \left(\mu_c C_{c,i} - \mu_c C_{c,j}\right)\left(\boldsymbol{E}_i - \boldsymbol{E}_j\right) \nabla W\left(\overrightarrow{r_{ij}}, h\right) - k_i \sum_{\kappa \in solid} \left(C_i - C_{eq}\right) \delta_{i\kappa} \tag{5}$$

and for the anion transport is

$$\frac{\mathrm{D}C_{a,i}}{\mathrm{D}t} = \sum_{j \in fluid} \frac{m_j \overrightarrow{r_{ij}}}{\rho_j \left(\overrightarrow{r_{ij}}\right)^2} \left(D_{a,i} + D_{a,j}\right)\left(C_{a,i} - C_{a,j}\right) \nabla W\left(\overrightarrow{r_{ij}}, h\right) + \sum_{j \in fluid} \frac{m_j \overrightarrow{r_{ij}}}{\rho_j \left(\overrightarrow{r_{ij}}\right)^2} \left(\mu_a C_{a,i} - \mu_a C_{a,j}\right)\left(\boldsymbol{E}_i - \boldsymbol{E}_j\right) \nabla W\left(\overrightarrow{r_{ij}}, h\right) \tag{6}$$

where m is the mass of the particle, ρ is the density of the particle, W is the SPH weighting function, h is the support length, and $\overrightarrow{r_{ij}}$ is the distance between particles i and j $(\overrightarrow{r_i} - \overrightarrow{r_j})$. $\sum_{j \in liquid}$ is a summation over all the fluid particles, $\sum_{\kappa \in solid}$ is a summation over all solid particles and

$$\delta_{i\kappa} = \begin{cases} 1, & \left|\overrightarrow{r_{ij}}\right| \le d \\ 0, & \left|\overrightarrow{r_{ij}}\right| > d. \end{cases} \tag{7}$$

$\delta_{i\kappa}$ ensures that the growth/dissolution occurs in a thin layer of thickness d (~8nm) at the fluid-solid interface and is approximately the thickness of the SEI layer[5]. The rate of mass change at the anode (solid phase) is equal to the rate of mass change in the electrolyte (liquid phase) and is described in Tartakovsky et al[17].
The Poisson equation discretization is

$$\Delta V_i = \frac{e\left(z_c C_{c,i} - z_a C_{a,i}\right)}{\epsilon_0 \epsilon} + \frac{1}{4\pi\epsilon_0\epsilon} \sum_j \frac{e\left(z_c C_{c,j} - z_a C_{a,j}\right)}{\overrightarrow{r_{ij}}}. \tag{8}$$

Outside of the diffusion layer, length L=35 μm, and initially (t=0) the concentration for both anions and cations is c_0 =0.5M and the electric field is constant, $\boldsymbol{E}_0$ = 8e-3 V μm^{-1}. Noise is introduced into the system by shifting the particles randomly (up to ±0.2*x, y spacing) from their initial ordered position.

C. Model Verification

The model presented is based on a previously verified precipitation/dissolution model and incorporates the additional electrochemical equations to track both the anion and cation species and the electrostatic potential. In order to verify these additions, two cases are considered. The first case calculates the ionic migration under a constant electric field and compares the model results and the results from a Runge-Kutta numerical solver to an analytical solution. In the second case, the Runge-Kutta method is compared to the SPH model as no analytical solution for the second case of ionic migration under a concentration-dependent electric field exists.

1) Case 1:

The 1-D governing equation of migration under constant electric field is

$$\frac{\delta c}{\delta t} = \mu \boldsymbol{E} \frac{\delta c}{\delta x} \tag{9}$$

where $0 > x > L = 1\mu$m, $\mu \boldsymbol{E} = 1\mu$m s^{-1}, and the initial concentration is given as

$$c(x, t = 0) = e^{-\frac{1}{2}\left(\frac{(x-\mu_m)}{\sigma}\right)^2} \tag{10}$$

where μ_m is 0.5 μm and σ^2 is 0.01 μm and the boundary conditions are

$$c(x = 0, t) = c(x = L, t) = 0, \tag{11}$$

and the analytical solution is

$$c(x, t) = e^{-\frac{1}{2}\left(\frac{((x+\mu \boldsymbol{E} t)-\mu_m)}{\sigma}\right)^2}. \tag{12}$$

2) Case 2:

The set of governing equations are (5 & 6) to track the anion and cation concentrations and the Poisson equation (2) to calculate the concentration-dependent electric field. The initial concentration for both species is

$$c_i(x, t = 0) = \frac{1}{2} erfc\left(\frac{x - \mu_m}{\sigma\sqrt{2}}\right) \tag{13}$$

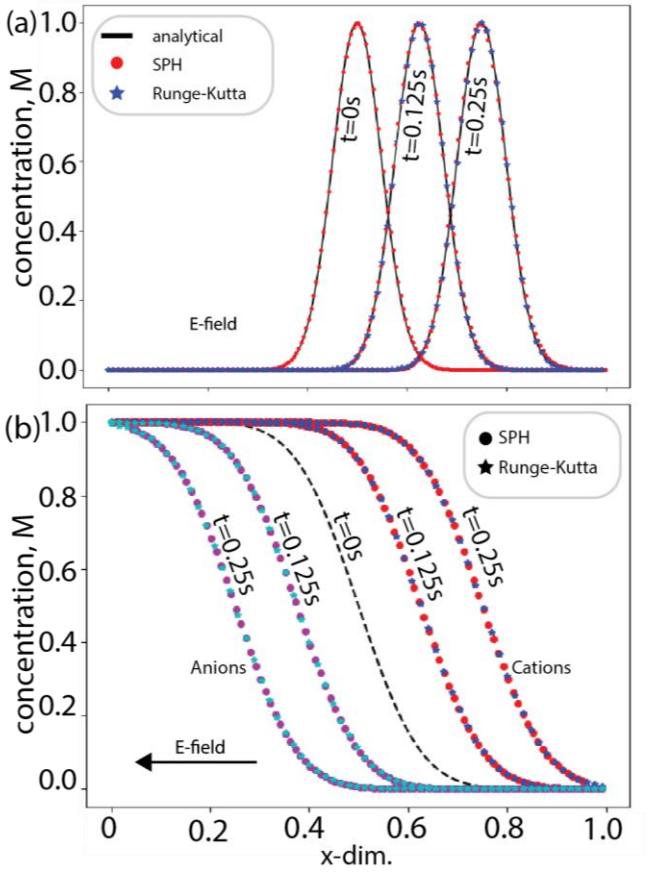

Figure 1. (a) Concentration profile for test case 1 where the migration is driven by a constant electric field and compares the results of the analytical solution, the SPH model and the Runge-Kutta method with an L1 average error of less 1%. (b) Concentration profile for test case 2 where the migration is driven by a concentration of both the anions and cations which are driven by a concentration-dependent electric field.

and the boundary conditions are $c_i(x = 0, t) = 1M$ and $c_i(x = L, t) = 0$.

With a SPH particle spacing of 0.02 μm for both Cases 1 and 2, the average L1 error is less than 1% for both cases. Comparison of the SPH, analytical and Runge-Kutta results are shown in Fig. 1.

III. Results and Discussion

A. Dendrite Morphology

The dendrite morphology is affected by which limiting factor is controlling deposition: reaction rate limited or mass transport limited. At higher charge rates, mass transport is the limiting factor and the lithium deposits favorably on breaks in the SEI layer leading to heterogenous, long, thin dendrite growth. At lower charge rates, the reaction rate at the anode is the limiting factor and lithium deposition is relatively smooth. These morphological outcomes have been observed experimentally. Dong et al used SEM imaging of the anode surface to observe the morphological differences between low (Fig. 2a) and high (Fig. 2b) charge rates[21]. Their experiments show that at lower current density, lithium deposition is relatively smooth with short, bushy dendrites. At high current density, lithium deposition is more heterogeneous and leads to longer, thinner dendrites.

Experimentally tracking Li^+ concentration and dendrite growth is difficult, so simulations are employed to garner further understanding of the phenomena near the anode surface. The diffusion-migration-reaction model simulates dendrite growth at the electrode-electrolyte interface (Fig. 3). An SEI layer with a single break is represented by a non-uniform reaction rate with a thickness of 8 nm at the anode surface. In Fig. 3a, the initial simulation domain is shown where the initial Li^+ concentration (0.5M) is the light green region, the grey region is the anode, the yellow region is the SEI layer with a reaction rate of 1 $\mu m\ s^{-1}$ and the red region

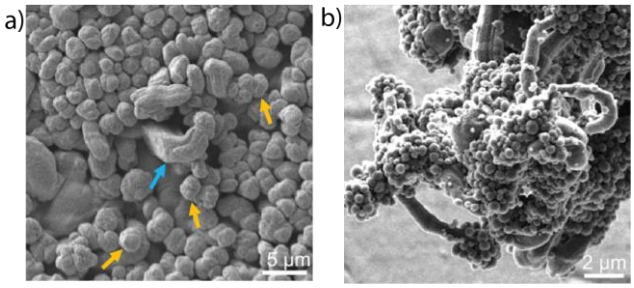

Figure 2. SEM images of lithium deposition at a low charge rate (a) and high charge rate (b). At the lower charge rate (a), lithium deposition forms uniformly as spherical structures along the anode surface. The blue arrow points to the non-spherical deposition regions and the orange arrows point to the more spherical depositions. At the higher charge rate (b), larger dendrites protrude from the anode surface and form longer thinner structures. Adapted with permission from Dong, K. et al Unravelling the Mechanism of Lithium Nucleation and Growth and the Interaction with the Solid Electrolyte Interface. Copyright (2021) American Chemical Society.

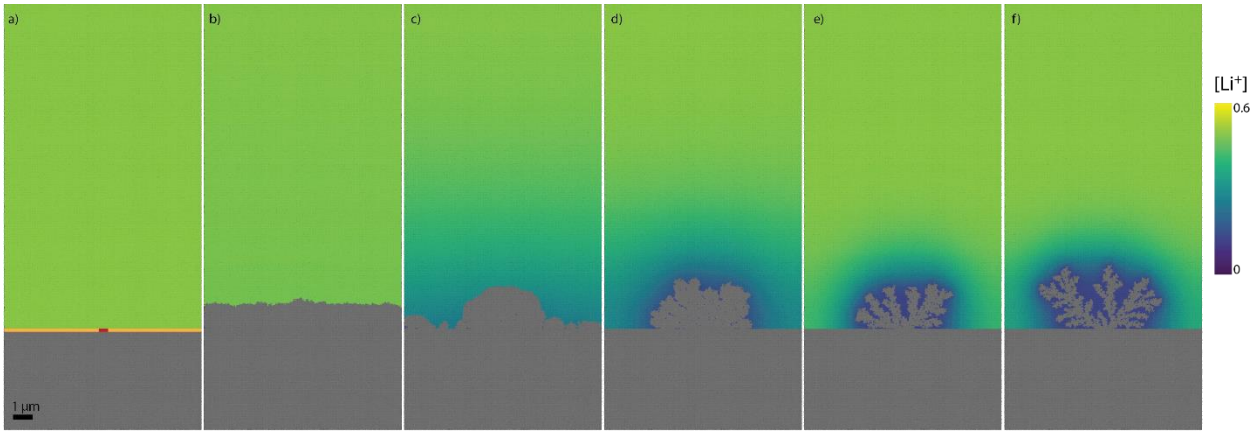

Figure 3. Simulation results after the first charge cycle. (a) is the initial setup where the grey region is the anode and the green region is the electrolyte. Along the surface of the anode there are two regions that have different reaction rates representing an SEI layer (yellow) and a break in the SEI (red). The break in the SEI has a higher reaction rate (1e4 μm s^{-1}) compared to the SEI layer (1 μm s^{-1}). (b) – (f) are simulations at the charge rates 0.01C, 0.1C, 1C, 5C and 7.5C, respectively. The electrolyte's cation concentration shows that at low charge rates, the concentration is higher near the anode surface leading to reaction rate limited dendrite growth. Also, the dendrite growth (grey) occurs more uniformly at lower charge rates. At high charge rates, dendrite growth is mass transport limited and dendrite growth only occurs at the break in the SEI layer.

represents the break in the SEI layer with a reaction rate of 1e4 $\mu m\ s^{-1}$. This investigation analyzed the cation concentration in regions surrounding the anode, the morphology of the dendrite growth and the local current density for five charge rates (Fig. 3b-f: 0.01C, 0.1C, 1C, 5C and 7.5C) after the first charge cycle.

At higher charge rates (Fig. 3d-f), the Li^+ concentration near the anode is depleted and the mass transport in the electrolyte becomes the limiting factor of lithium deposition. Although lithium is initially deposited on the entire surface of the anode, it is more favorably deposited on the break in the SEI layer. Once this region begins to form a dendrite, it is able to access regions in the electrolyte with higher Li^+ concentrations. This leads to further dendrite growth and creates longer, thinner structures as expected. This growth morphology creates high current density at the tips of the dendrites (Fig. 4c). High current density leads to the breakdown of the electrolyte and reduces the columbic efficiency of the battery. Additionally, dendrites that grow long enough can pierce the battery separator causing short circuits and battery failure. Even though these faster charge rates are desirable, they create unsafe operating conditions.

At lower charge rates (Fig. 3b,c), the Li^+ concentration is higher in the region surrounding the anode. This occurs because the reaction rate is the limiting factor of the lithium deposition on the anode surface. This deposition morphology is more uniform and occurs despite breaks in the SEI layer. There is a more uniform current density for this deposition morphology as well (Fig.4a). Ideally, the limiting factor should be the charge rate which allows the battery to be operated safely. However, for this condition to be met, the battery takes longer to charge. One possible method for faster charging involves modifying the surface geometry of the anode and is explored in the last section of this work.

B. Local Current Density

Experimentally, it is difficult to verify and observe the effects of local variation in current density. However, with the Nernst-Plank equations implemented into the SPH model, the effect of local current density on dendrite growth can be observed (Fig. 4). The current density J at the anode surface is calculated as

$$\frac{-J}{z_c e} = D_c \Delta c_c + \mu_c c_c \nabla \boldsymbol{E}. \tag{14}$$

Fig. 4 illustrates the local current density along the anode/dendrite interface at three charge rates. The current density is most uniform at the 0.01C charge rate and least uniform at the 7.5C charge rate. High current density is related to faster mass transport causing longer, thinner dendrite growth. As the long, thin dendrites protrude further from the original anode surface, they have access to regions with greater cation concentrations and are in a stronger electric

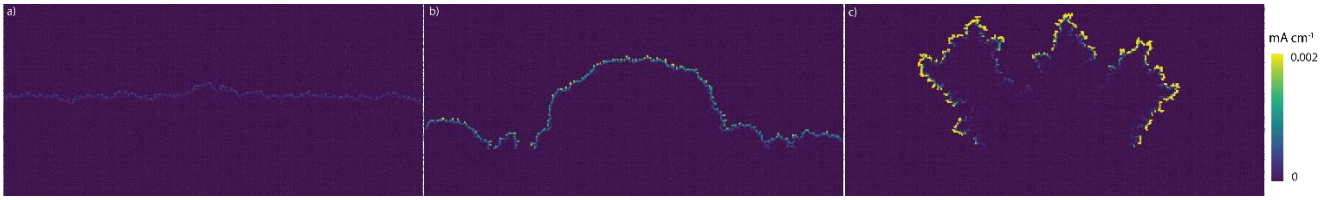

Figure 2. Local current density for (a) 0.01C, (b) 0.1C, and (c) 7.5C charge rates after the first charge cycle. Higher current density equates to higher surface overpotentials and faster mass transport. This leads to problematic dendrite growth.

field further accelerating dendrite growth, creating a positive feedback loop. This dendrite morphology has the potential to pierce the separator leading to catastrophic battery failure.

C. *Surface geometry*

Kim et al conducted experiments to understand how modifying the surface geometry can effect dendrite morphology at a single charge rate. They used a mold to create an impression on the anode surface. To further explore this method for faster charging scenarios, simulations were conducted at high and low charging rates. A schematic of the altered surface geometry simulations is presented in Fig. 5 where the green region is the electrolyte, the grey region is the anode, the yellow region is the native SEI layer, and the red region is the broken SEI layer (higher reaction rate). The dimensions of the surface geometry are 1.2 μm by 6 μm and match those of Kim et al[11].

The results from Kim et al's experimental tests (top row) and the SPH simulations are presented in Fig. 6. The middle row is the low charge rate (0.1C), the bottom row is high charge rate (1C), the left column is the flat anode surface and the right column is the altered anode surface. From Fig. 6, we see that the deposition is uniform at the low charge rates for both the smooth and the altered anode surface. However, as the surface area increases, i.e. not flat, the area for lithium deposition increases leading to a lower total current density at the same charge rate. This creates safer operating conditions for the battery.

At the higher charge rate and flat anode surface (Fig. 6e), we begin to see that the lithium deposition is heterogeneous. This heterogeneity is caused by some regions consuming the local Li^+ leaving the surrounding regions starved.

There are two deposition morphologies when the anode surface is altered (Fig. 6f). The deposition is non-uniform along the top edge of the impression where the native SEI remains. In this region, dendrites form, particularly at the corner of the impression. The dendrite formation along the top surface in Fig. 6f resembles the dendrite formation in Fig. 6e, which is expected as these surfaces both are covered in the native SEI layer. Along the bottom surface of the impression where the SEI layer has been broken, Li^+ deposits much more uniformly as compared to the top surface. One possible reason for this is that the bottom surface has access to greater amounts of Li^+ in the impression. If the reactive surface has access to greater Li^+ concentrations, the limiting factor for the reaction will be the reaction rate and not mass transport leading to a more uniform deposition.

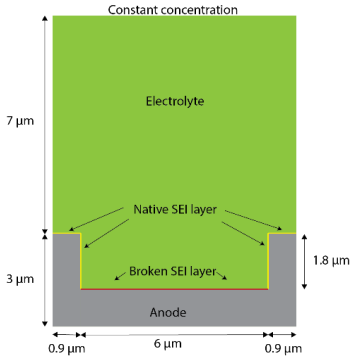

Figure 3. Schematic of the simulation domain for the altered surface geometry. Along the top is a constant lithium concentration boundary condition in the electrolyte (green) farther from the anode (grey) and the native SEI layer (yellow) and the broken SEI layer (red) are at the anode-electrolyte interface.

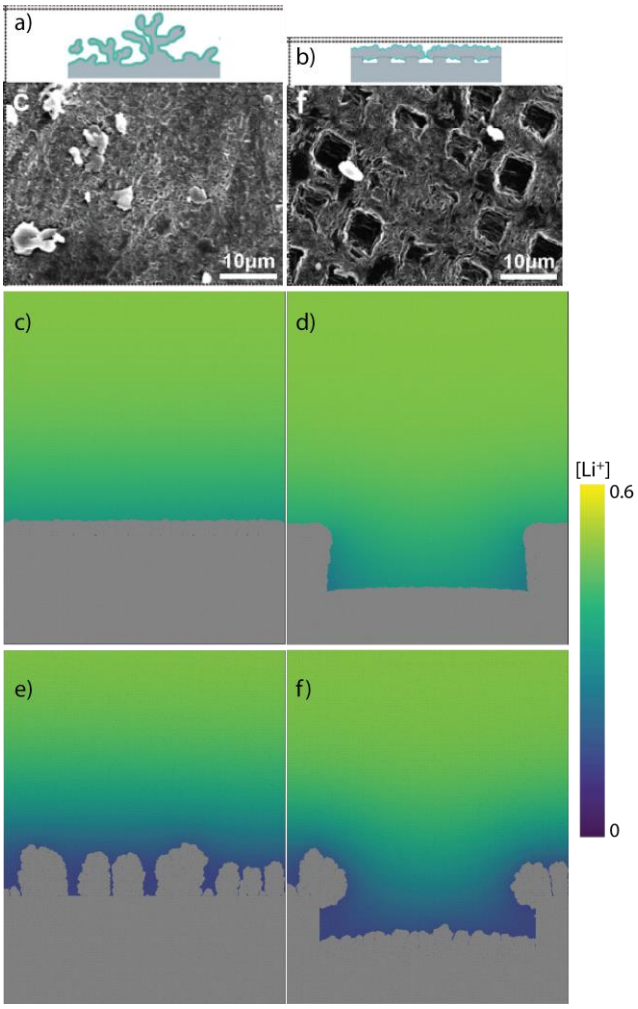

Figure 4. The results from Kim et al's experimental work (top row) and the simulations of a low (0.1C, middle row) and high (1C, bottom row) charge rate for a flat (left column) and altered (right column) anode geometry. Adapted with permission from Y.-J. Kim et al. ChemElectroChem ***2018***, 5, *3169. Copyright (2018) ChemElectroChem.*

IV. Conclusions

An SPH model of diffusion, migration and reactive surfaces has been developed to understand the complex phenomena of dendrite growth at the electrode-electrolyte interface of a lithium metal battery. Verification of the migration and electrostatic equations demonstrate the model's ability to accurately simulate the electrochemical physics. The model's dendrite morphology qualitatively matches with that of experimental observations. The morphology of the dendrite growth is controlled by several factors such as charge rate, cation concentration near the anode surface, SEI layer

uniformity and non-uniform current densities along the anode surface.

Increasing the charge rate is desirable for faster battery charging but comes at the cost of dendritic growth. The high current density at the tips of dendrites can lead to a host of problems like the further breakdown of the SEI and the electrolyte. One possible method for reducing high local current density without reducing the charge rate could be to modify the surface geometry of the anode. Modifying the surface geometry also leads to a more uniform lithium deposition. The modified surface geometry creates regions in the electrolyte that act as reserves of Li^+ for the bottom surface of the impression. This reserve prevents mass transport from being the limiting factor of the reaction leading to a more uniform deposition of lithium. Future work will explore a more intentional approach to selecting the geometry to impress upon the anode surface.

ACKNOWLEDGEMENT

This research is supported by the National Science Foundation under Grant No. 2034154.

REFERENCES

[1] Goodenough, J. B.; Park, K. S. The Li-Ion Rechargeable Battery: A Perspective. *Journal of the American Chemical Society*. 2013. https://doi.org/10.1021/ja3091438.

[2] Lin, D.; Liu, Y.; Cui, Y. Reviving the Lithium Metal Anode for High-Energy Batteries. *Nature Nanotechnology*. 2017. https://doi.org/10.1038/nnano.2017.16.

[3] Chen, Q.; Geng, K.; Sieradzki, K. Prospects for Dendrite-Free Cycling of Li Metal Batteries. *J. Electrochem. Soc.* **2015**. https://doi.org/10.1149/2.0261510jes.

[4] Li, N.; Wei, W.; Xie, K.; Tan, J.; Zhang, L.; Luo, X.; Yuan, K.; Song, Q.; Li, H.; Shen, C.; Ryan, E. M.; Liu, L.; Wei, B. Suppressing Dendritic Lithium Formation Using Porous Media in Lithium Metal-Based Batteries. *Nano Lett.* **2018**. https://doi.org/10.1021/acs.nanolett.8b00183.

[5] Nojabaee, M.; Küster, K.; Starke, U.; Popovic, J.; Maier, J. Solid Electrolyte Interphase Evolution on Lithium Metal in Contact with Glyme-Based Electrolytes. *Small* **2020**, *16* (23), 1–5. https://doi.org/10.1002/smll.202000756.

[6] Yoon, I.; Jurng, S.; Abraham, D. P.; Lucht, B. L.; Guduru, P. R. Measurement of Mechanical and Fracture Properties of Solid Electrolyte Interphase on Lithium Metal Anodes in Lithium Ion Batteries. *Energy Storage Mater.* **2020**, *25* (September 2019), 296–304. https://doi.org/10.1016/j.ensm.2019.10.009.

[7] Jurng, S.; Brown, Z. L.; Kim, J.; Lucht, B. L. Effect of Electrolyte on the Nanostructure of the Solid Electrolyte Interphase (SEI) and Performance of Lithium Metal Anodes. *Energy Environ. Sci.* **2018**, *11* (9), 2600–2608. https://doi.org/10.1039/c8ee00364e.

[8] Ely, D. R.; García, R. E. Heterogeneous Nucleation and Growth of Lithium Electrodeposits on Negative Electrodes. *J. Electrochem. Soc.* **2013**. https://doi.org/10.1149/1.057304jes.

[9] Ramasubramanian, A.; Yurkiv, V.; Foroozan, T.; Ragone, M.; Shahbazian-Yassar, R.; Mashayek, F. Stability of Solid-Electrolyte Interphase (SEI) on the Lithium Metal Surface in Lithium Metal Batteries (LMBs). *ACS Appl. Energy Mater.* **2020**, *3* (11), 10560–10567. https://doi.org/10.1021/acsaem.0c01605.

[10] Wood, K. N.; Kazyak, E.; Chadwick, A. F.; Chen, K. H.; Zhang, J. G.; Thornton, K.; Dasgupta, N. P. Dendrites and Pits: Untangling the Complex Behavior of Lithium Metal Anodes through Operando Video Microscopy. *ACS Cent. Sci.* **2016**. https://doi.org/10.1021/acscentsci.6b00260.

[11] Kim, Y. J.; Jin, H. S.; Lee, D. H.; Choi, J.; Jo, W.; Noh, H.; Lee, J.; Chu, H.; Kwack, H.; Ye, F.; Lee, H.; Ryou, M. H.; Kim, H. T. Guided Lithium Deposition by Surface Micro-Patterning of Lithium-Metal Electrodes. *ChemElectroChem* **2018**, *5* (21), 3169–3175. https://doi.org/10.1002/celc.201800694.

[12] Zhang, X.; Zou, L.; Xu, Y.; Cao, X.; Engelhard, M. H.; Matthews, B. E.; Zhong, L.; Wu, H.; Jia, H.; Ren, X.; Gao, P.; Chen, Z.; Qin, Y.; Kompella, C.; Arey, B. W.; Li, J.; Wang, D.; Wang, C.; Zhang, J. G.; Xu, W. Advanced Electrolytes for Fast-Charging High-Voltage Lithium-Ion Batteries in Wide-Temperature Range. *Adv. Energy Mater.* **2020**, *10* (22). https://doi.org/10.1002/aenm.202000368.

[13] Du, Z.; Wood, D. L.; Belharouak, I. Enabling Fast Charging of High Energy Density Li-Ion Cells with High Lithium Ion Transport Electrolytes. *Electrochem. commun.* **2019**, *103*, 109–113. https://doi.org/10.1016/J.ELECOM.2019.04.013.

[14] Keil, P.; Jossen, A. Charging Protocols for Lithium-Ion Batteries and Their Impact on Cycle Life-An Experimental Study with Different 18650 High-Power Cells. *J. Energy Storage* **2016**. https://doi.org/10.1016/j.est.2016.02.005.

[15] Monaghan, J. J. Smoothed Particle Hydrodynamics. *Reports on Progress in Physics*. 2005. https://doi.org/10.1088/0034-4885/68/8/R01.

[16] Gao, L.; Guo, Z. Phase-Field Simulation of Li Dendrites with Multiple Parameters Influence. *Comput. Mater. Sci.* **2020**. https://doi.org/10.1016/j.commatsci.2020.109919.

[17] Tartakovsky, A. M.; Meakin, P.; Scheibe, T. D.; Eichler West, R. M. Simulations of Reactive Transport and Precipitation with Smoothed Particle Hydrodynamics. *J. Comput. Phys.* **2007**. https://doi.org/10.1016/j.jcp.2006.08.013.

[18] Tan, J.; Cannon, A.; Ryan, E. Simulating Dendrite Growth in Lithium Batteries under Cycling Conditions. *J. Power Sources* **2020**, *463*, 228187. https://doi.org/https://doi.org/10.1016/j.jpowsour.2020.228187.

[19] Chazalviel, J. N. Electrochemical Aspects of the Generation of Ramified Metallic Electrodeposits. *Phys. Rev. A* **1990**. https://doi.org/10.1103/PhysRevA.42.7355.

[20] Tan, J.; Ryan, E. M. Computational Study of Electro-Convection Effects on Dendrite Growth in Batteries. *J. Power Sources* **2016**. https://doi.org/10.1016/j.jpowsour.2016.05.012.

[21] Dong, K.; Xu, Y.; Tan, J.; Osenberg, M.; Sun, F.; Kochovski, Z.; Pham, D. T.; Mei, S.; Hilger, A.; Ryan, E.; Lu, Y.; Banhart, J.; Manke, I. Unravelling the Mechanism of Lithium Nucleation and Growth and the Interaction with the Solid Electrolyte Interface. **2021**. https://doi.org/10.1021/acsenergylett.1c00551.